

# Formalizing and Estimating Distribution Inference Risks

Anshuman Suri and David Evans  
Department of Computer Science  
University of Virginia  
{anshuman, evans}@virginia.edu

**Abstract**—Property inference attacks reveal statistical properties about a training set but are difficult to distinguish from the intrinsic purpose of statistical machine learning, namely to produce models that capture statistical properties about a distribution. Motivated by Yeom et al.’s membership inference framework, we propose a formal and general definition of property inference attacks. The proposed notion describes attacks that can distinguish between possible training distributions, extending beyond previous property inference attacks that infer the ratio of a particular type of data in the training data set such as the proportion of females. We show how our definition captures previous property inference attacks as well as a new attack that can reveal the average node degree or clustering coefficient of a training graph. Our definition also enables a theorem that connects the maximum possible accuracy of inference attacks distinguishing between distributions to the effective size of dataset leaked by the model. To quantify and understand property inference risks, we conduct a series of experiments across a range of different distributions using both black-box and white-box attacks. Our results show that inexpensive attacks are often as effective as expensive meta-classifier attacks, and that there are surprising asymmetries in the effectiveness of attacks. We also extend the state-of-the-art property inference attack to work on convolutional neural networks, and propose techniques to help identify parameters in a model that leak the most information, thus significantly lowering resource requirements for meta-classifier attacks.

## I. INTRODUCTION

Inference attacks seek to infer sensitive information about the training process of a revealed machine-learned model, most often about the training data. For example, in a membership inference attack [1], the adversary aims to infer whether a particular datum was part of the training data. In a property inference attack, an adversary aims to infer some statistical property of the training dataset, such as the proportion of women in a dataset used to train a smile-detection model [2].

The privacy threat posed by membership inference attacks is apparent—if an adversary can infer the presence of a particular user record in a training dataset of diabetes patients, it would violate privacy laws limiting medical disclosure. Property inference attacks pose a less apparent threat but can also be dangerous. Consider an organization that trains a graph neural network on graph data based on the topology of their servers and publishes this model. Assume some adversary wants to insert a botnet (a group of malicious nodes) into the victim’s network without raising suspicion. Suppose the adversary infers the effective diameter (90<sup>th</sup> percentile of all pair-wise shortest paths) of the underlying graph just via access to the model (Figure 1). Even though this property is not

inherently valuable, many botnet-detection systems rely on such properties as features [3]. Thus, the adversary could carefully craft botnets to match the effective diameter of the graph, making detection harder for botnet-detection systems.

The research community lacks a good understanding of property inference attacks—for example, different notions are used in [4], [5], [6]. Many formal privacy notions have been proposed, including numerous variations on differential privacy, but most focus on protecting specific data elements, not the statistical properties of a dataset. One notable exception is the Pufferfish framework [7], which introduces notions that allow capturing aggregates of records via explicit specifications of potential secrets (e.g., distribution of vehicle routes in a shipping company) and their relations. Although the Pufferfish framework supports aggregate secrets, it is unclear how it can be extended to support distribution-level properties.

In all previous work on property inference attacks, the target property has been distinguishing between ratios of training data satisfying a particular attribute or quality, like an individual’s sex in face images. Along these lines, a recent attempt to formalize property inference [8] consists of a framework that reduces property inference to Boolean functions of individual members, posing the ratio of members satisfying the given function in a dataset as the property. The broad idea for all methods for property inference attacks in the literature so far is to use meta-classifiers: the adversary trains models on datasets with different properties, then trains a meta-classifier for property inference using model representations from those models. The adversary then uses the meta-classifier to look at the victim’s model and predict a property of

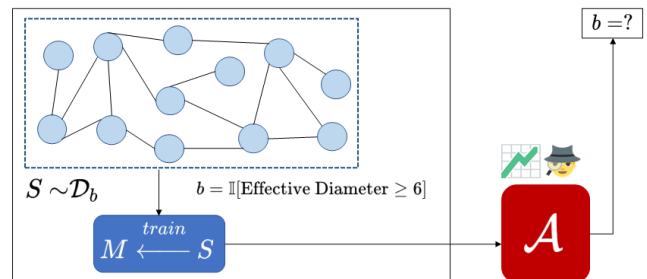


Fig. 1: Information flow in an example of property inference attack. The adversary seeks information about some underlying distribution via access to a model trained on a dataset sampled from that distribution.

the model’s training data. These model representations can take several forms: using model weights themselves with permutation-invariance [9], or model activations or logits for a static/dynamically-generated set of query points [10]. These methods show promise, achieving better-than-random results for several properties, various tasks, and models across different domains. For instance, predicting a doctor’s specialty based on rating-prediction systems on text reviews [6], identifying accents of speakers in voice-recognition models [2], and even predicting if a model has been trained to have a backdoor Trojan [10]. Although these approaches achieve high accuracy rates on classifiers like decision trees and shallow neural networks, successful property inference attacks have not been demonstrated on relatively large deep neural networks or complex datasets. Training deep learning models with multiple layers (including convolutional neural networks) is much more time-consuming than simpler machine learning models. Such models’ large parameters mean many more local classifiers are needed to train an effective meta classifier [11].

Moreover, ratio-based formulations limit the threat model since it cannot capture many other kinds of statistical properties of the training distribution that may be sensitive, like the degree distribution of a graph [12]. In this work, we formalize property inference attacks based on a critical insight: the key difference between property inference attacks and other inference attacks is that the adversary’s goal in the former is to learn about the training *distribution*, not about the specific training *dataset*. Dataset inference attacks, such as membership inference [1], attribute inference [13], and ownership-resolution [14] operate on the level of training records. Attacks like membership inference are directly connected to differential privacy which bounds the ability to distinguish neighboring datasets. By contrast, distribution inference attacks attempt to learn statistical properties of the underlying distribution from which the training dataset is sampled.

*Related Works.* Training large models involve randomness in many places: weight initialization, the order of batches, and dropout, to name a few. This stochasticity makes it hard to assert whether two models were trained on similar datasets or not. Recent attacks on hyper-parameter stealing [15] along with practical attacks on huge real-world language models [16] suggest there might be some way to infer dataset properties for deep-learning models. However, questions like the feasibility of such attacks on these models or even what kinds of properties an adversary should infer remain unanswered. We demonstrate the capability of such attacks to work on large convolutional networks and different datasets across domains. However, it is unknown how well such attacks (using existing techniques) can work on even larger models or across different domains.

A natural extension of our definition would incorporate a poisoning opportunity where the adversary can participate in the training process itself. Such an adversary may poison the training dataset by injecting adversarially crafted datapoints (explored in the literature [8]) or control the training procedure itself to introduce some Trojan in the model. Recent works

look at a similar scenario where the adversary participates in the learning process via a federated-learning setup, launching attribute-reconstruction attacks using epoch-averaged model gradients [17].

**Contributions.** We propose a general and straightforward experiment to formalize property inference attacks, inspired by Yeom *et al.*’s membership inference definition [18] (Section II). Our definition is generic enough to capture any statistical property of the underlying distribution, including, but not limited to, the attribute ratios that have been the focus of previous property inference attacks. Using the definition, we prove a theorem that gives a way to compare effectiveness of property inference attacks across different distributions via the size of the effective training set  $n_{\text{effective}}$ , for the case of ratios of binary functions as properties. The theorem allows us to derive the effective size of the dataset leaked by the model through a property inference attack.

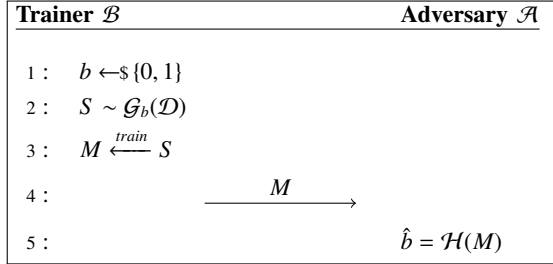
We report on experiments evaluating property inference is a risk across several datasets and properties, providing the first systematic evaluation of how property inference risks vary as distributions to distinguish diverge. To conduct our experiments we introduce two simple black-box property inference attacks, and extend the white-box permutation-invariant network [9] architecture, the current state-of-the-art property inference method, to add support for convolutional layers (Section III). This enables us to conduct property inference attacks on deep-neural networks, even when the target models are trained from scratch.

Simple black-box attacks perform surprisingly well for many of the ratios across multiple datasets, while exhibiting asymmetry in performance (where it is expected theoretically) as distributions diverge from each other. (Section IV-B). We also observe this asymmetry while varying the similarity between distributions simultaneously (Section IV-C). We analyze the information picked up by meta-classifiers across layers, finding that some layers are more informative than the others while distinguishing between certain properties (Section V). Motivated by these observations, we propose a method to rank and identify layers based on the information they leak about underlying distributions. This enables meta-classifier attacks that might otherwise be prohibitively expensive by only using parameters from an identified subset of model layers without compromising accuracy.

## II. FORMALIZING PROPERTY INFERENCE

Let  $\mathcal{D} = (\mathcal{X}, \mathcal{Y})$  be a public distribution between data,  $\mathcal{X}$ , and its corresponding labels,  $\mathcal{Y}$ . We assume both the model trainer  $\mathcal{B}$  and adversary  $\mathcal{A}$  have access to  $\mathcal{D}$ . Both parties also have access to two functions  $\mathcal{G}_0, \mathcal{G}_1$  that transform distributions. Inferring properties of the distribution can reveal sensitive information in many scenarios, which can be captured by suitable choices of  $\mathcal{G}_0$  and  $\mathcal{G}_1$ . We use these functions  $\mathcal{G}_0, \mathcal{G}_1$  instead of directly mentioning two distributions  $\mathcal{D}_0, \mathcal{D}_1$  to stress the fact that the resulting distributions  $\mathcal{G}_0(\mathcal{D}), \mathcal{G}_1(\mathcal{D})$  are transformations of  $\mathcal{D}$ , not just any two arbitrary distributions.

In our cryptographic game definition,  $\mathcal{B}$  picks one of these distribution transformers at random and samples a dataset  $S$  from the resulting distribution. Given access to a model  $M$  trained on  $S$ , the adversary aims to infer which of the two distribution mappers,  $\mathcal{G}_0$  or  $\mathcal{G}_1$ , was used. The property inference experiment can be described as:



If  $\mathcal{A}$  can successfully predict  $b$  via  $\hat{b}$ , then it can determine which of the two properties the training distribution satisfied. The advantage of the adversary  $\mathcal{A}$  using algorithm  $\mathcal{H}$  is:

$$\text{Adv}_{\mathcal{H}} = \left| \Pr[\hat{b} = b] - \Pr[\hat{b} \neq b] \right|.$$

This advantage is negligible when the adversary does no better than random guessing. In this work, we assume the adversary has no control over the training process.

**Applying the Definition to Previous Attacks.** Seminal works on property inference [2], [9] involve a model trained either on the original dataset or a version modified to be biased towards some chosen attribute. Our definition can be used to describe these attacks by setting  $\mathcal{G}_0$  to the identity function (so  $\mathcal{G}_0(\mathcal{D})$  is original distribution  $\mathcal{D}$ ) and  $\mathcal{G}_1$  to a filter that adjusts the distribution to have a specified ratio over the desired attribute. With respect to a binary property function,  $f : \mathcal{X} \rightarrow \{0, 1\}$ ,  $\mathcal{D}$  can be characterized using a generative probability density function:

$$\rho_{\mathcal{D}}(\mathbf{x}) = \sum_{c \in \{0,1\}} p(c) \cdot p(\mathbf{x} | c), \quad (1)$$

where  $p(c)$  is a multinomial distribution representing the probabilities over the desired (binary) property function  $f$  and its possible values  $c$ , and  $p(\mathbf{x} | c)$  is the generative conditional probability density function. Then,  $\mathcal{G}_1(\mathcal{D})$  can be expressed using the following probability density function, with an adjusted prior  $\hat{p}$ :

$$\rho_{\mathcal{G}_1(\mathcal{D})}(\mathbf{x}) = \sum_{c \in \{0,1\}} \hat{p}(c) \cdot p(\mathbf{x} | c), \quad \hat{p}(1) = \alpha, \quad \hat{p}(0) = 1 - \alpha \quad (2)$$

where  $\alpha$  is the probability of a randomly sampled point satisfying the property function  $f$ . Thus, a uniformly randomly sampled dataset from  $\mathcal{G}_1(\mathcal{D})$  would have an expected ratio of  $\alpha$  of its members satisfying  $f$ . Additionally, we can modify  $\mathcal{G}_0$  with a similarly adjusted prior, enabling the adversary to distinguish between any two arbitrary ratios [6].

The maximum distinguishing accuracy that an adversary can hope to achieve while inferring ratio-related properties can be upper bounded based on the ratios themselves and the effective

size of the recovered data set, given by the theorem below which is proven in Appendix B.

**Theorem II.1.** For two distributions  $\mathcal{G}_0(\mathcal{D})$ ,  $\mathcal{G}_1(\mathcal{D})$  with prior values  $\alpha_0, \alpha_1$  derived from the same underlying distribution  $\mathcal{D}$ , the distinguishing accuracy between models trained on datasets of size  $n$  from these distributions is at most

$$\frac{1}{2} + \frac{\min \left\{ \sqrt{1 - \left( \frac{\min(\alpha_0, \alpha_1)}{\max(\alpha_0, \alpha_1)} \right)^n}, \sqrt{1 - \left( \frac{1 - \max(\alpha_0, \alpha_1)}{1 - \min(\alpha_0, \alpha_1)} \right)^n} \right\}}{2}.$$

This upper bound is proportional to the difference in priors, which is intuitive—distributions with a larger difference in ratios can be seen as “more different” and thus easier to distinguish. It captures the notion of an adversary being able to perfectly reconstruct a sample dataset of effective size  $n$  from the model’s training distribution (at least with respect to the inferred property).

For the datasets we experiment with, these bounds correspond to near-perfect distinguishing accuracy if the full training dataset was recovered by the adversary in nearly all cases. Experimentally, the value of  $n$  corresponding to the observed distinguishing performance, which we term  $n_{\text{effective}}$ , is a useful way to quantify a given method’s capabilities in terms of retrieving information about a given model’s training dataset. We plot observed performance for some of our experiments in Figure 2 to show how these trends change with values of  $n_{\text{effective}}$ , as well the ratios themselves. The results show that the most effective property inference attacks for all datasets (other than RSNA Bone Age) are less accurate predictors than would be possible from a random sample of size two from the training distribution. This shows how little information the model is leaking relative to its actual training set size (1800 for Census (race), the smallest of them), but that this is still enough for accurate property inference predictions when the distributions are different enough

### III. ATTACKS

In our experiments to evaluate the risks of property inference attacks, we use two simple black-box attacks and the state-of-the-art white-box meta-classifier attack based on Permutation-Invariant Networks [9]. We extend the meta-classifier attack to support convolutional neural networks (Section III-B2).

#### A. Black-Box Attacks

The black-box attacks assume the adversary has access to representative data for the candidate distributions, but only has API access to the target model which outputs its prediction for a submitted input.

1) *Loss Test:* A simple algorithm  $\mathcal{H}$  consists of using the accuracy, or any other metric used while training the model  $M$ , to compute  $\hat{b}$ . For samples of data  $S_{b \in \{0,1\}} \sim \mathcal{G}_b(\mathcal{D})$ :

$$\hat{b} = \mathbb{I}[\text{acc}(M, S_0) < \text{acc}(M, S_1)], \quad (3)$$

where  $\text{acc}(M, S)$  is the accuracy of model  $M$  on some sample of data  $S$ , and  $\mathbb{I}$  is the indicator function. Intuitively, a model would have higher accuracy on data sampled from the training

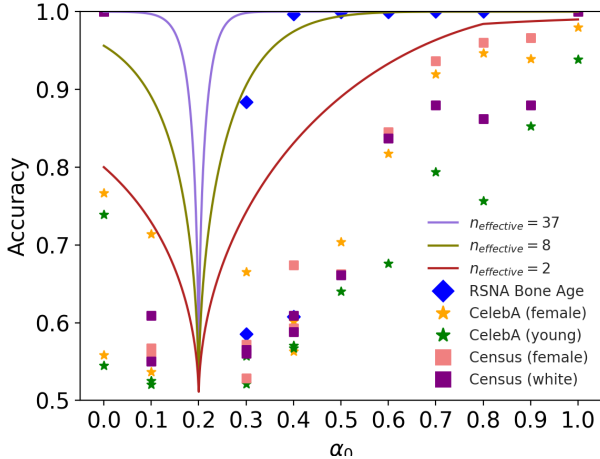


Fig. 2: Distinguishing accuracy for  $\alpha_1 = 0.2$  according to the upper bound for  $n_{\text{effective}}$  for datasets with this  $\alpha_1$ , along with maximum accuracies (across all attacks and runs) for RSNA Bone Age, Census, and CelebA. Curves corresponding to actual dataset sizes indicate near-perfect distinguishing accuracies in all cases. Hollow points correspond to  $(1 - \alpha_0, 0.8)$ , since they have the same upper bound as  $(\alpha_0, 0.2)$ . Results are for the most effective attacks from the experiments described in Section IV.

distribution, compared to another distribution. This method does not require the adversary to train models, but only to have access to suitable test distributions, and the ability to submit samples from those distributions to the target model.

2) *Threshold Test*: The Loss Test assumption may not hold for some pairs of properties if one distribution is inherently easier to classify than the other (as we observe in our experiments in Section IV-B). To account for this, we consider an attack where the adversary uses a small (balanced) sample of models from each distribution to identify which of  $S_0$  or  $S_1$  maximizes the performance gap between its models.

$$\gamma_{b \in \{0,1\}} = \sum_{i: y_i=0} \text{acc}(M^i, S_b) - \sum_{i: y_i=1} \text{acc}(M^i, S_b)$$

$$k = \mathbb{I}[|\gamma_0| < |\gamma_1|], \quad (4)$$

where  $y_i = b$  denotes that the model  $M^i$  is trained on a dataset sampled from  $\mathcal{G}_b(\mathcal{D})$ . After identifying  $k_{\in \{0,1\}}$ , the adversary derives a threshold  $\lambda$  to maximize accuracy distinguishing between models trained on datasets from the two distributions (using a simple linear search). Assuming  $\gamma_k$  is positive,

$$\delta(\Lambda) = \sum_{i: y_i=0} \mathbb{I}[\text{acc}(M^i, S_k) \geq \Lambda] + \sum_{i: y_i=1} \mathbb{I}[\text{acc}(M^i, S_k) < \Lambda]$$

$$\lambda = \arg \max_{\Lambda} \delta(\Lambda). \quad (5)$$

The prediction  $\hat{b}$  is then computed as:  $\hat{b} = \mathbb{I}[\text{acc}(M, S_k) \geq \lambda]$  (or with a  $<$  inequality when  $\gamma_k$  is negative). Thus, the adversary uses a sample of locally-trained models to derive a classification

rule based on model accuracy, which it then uses to infer the training distribution of the target model.

### B. White-Box Attacks

The white-box attacks assume that the adversary has direct access to the victim model, including its parameters, and has access to a sufficiently large amount of representative data to train local models on the candidate distributions.

1) *Meta-Classifiers*: The state-of-the-art property inference attack is Ganju et al.'s attack using Permutation-Invariant Networks as meta-classifiers [9]. The meta-classifiers take as input model parameters (weights, bias) and predict which distribution was used to sample training data for the model. This architecture is designed to be invariant to different neuron orderings inside neural network layers, which it achieves by utilizing the DeepSets [19] architecture. Neuron-ordering invariance is achieved via a set of transforming functions,  $\phi_i$  (defined for each layer  $i$ ), over each row of the layer weight matrix. The outputs of these functions are then summed to create a layer representation  $L^i$ , achieving invariance to the ordering of the neurons within each layer via the summation function. Since the meta-classifier is itself a classifier that requires many models (800 per distribution, based on how many models the original Permutation-Invariant Networks used) trained on the two distributions for training, this attack is only feasible for adversaries with access to sufficient data from both training distributions and considerable computational resources.

2) *Targeting Convolutional Neural Networks*: The Permutation-Invariant Network only supports linear layers in a feed-forward architecture and has been explored in previous work only with two-three layer MLPs on small datasets [9], or single-layer recurrent neural networks [6]. We extend property inference attacks to convolutional neural networks, demonstrating their effectiveness on deep-learning models trained from scratch.

Figure 3 illustrates our method. Let  $K$  be a kernel of size  $(k_1, k_2)$  associated with some convolutional layer, with input and output channel dimensions  $c_{in}$  and  $c_{out}$  respectively. While designing the architecture to capture invariance, it is important to remember that positional information in the kernel matters, unlike neurons in a linear layer. Thus, any attempt to capture invariance should be limited to the mapping between input and output channels of a convolutional kernel. With this in mind, we flatten the kernel from four dimensions  $(k_1, k_2, c_{in}, c_{out})$  to two, such that the resulting matrix is of size  $(k_1 \times k_2 \times c_{in}, c_{out})$ . Concatenating along the input channel dimension helps preserve location-specific information learned by the kernel while capturing permutation invariance across the output channels themselves.

This two-dimensional matrix is then processed in the same way as the linear layers are in permutation-invariant networks, applying function  $\phi_i$  and summing across output dimension to capture invariance while concatenating feature representations from prior layers. Similarly to the original architecture, the bias component can be concatenated to the kernel matrix itself. Since this feature extraction process on a convolutional

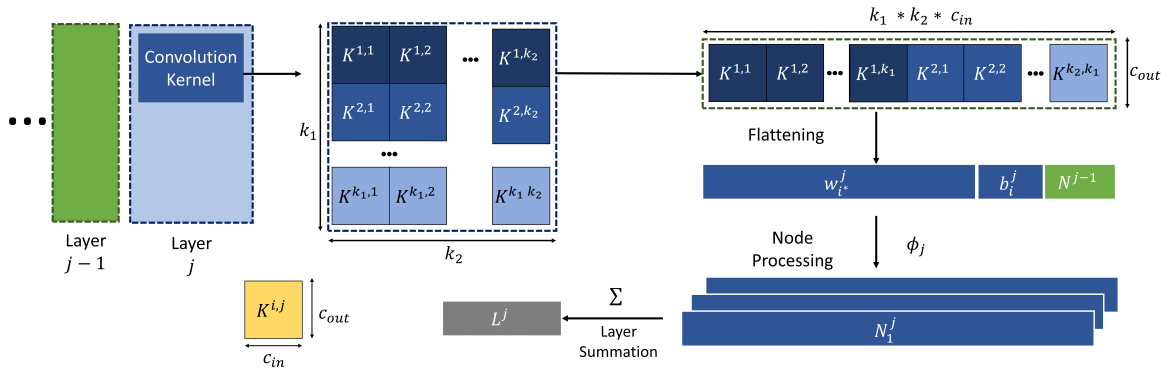


Fig. 3: Transforming a  $k_1 \times k_2$  kernel matrix  $K$  (with input channels  $c_{in}$  and output channels  $c_{out}$ ) into a 2-dimensional weight matrix for compatibility with the Permutation Invariant Network architecture.

layer also produces a layer representation, it can be easily incorporated into the existing architecture to work on models with a combination of convolutional and linear layers.

#### IV. EXPERIMENTS

We execute property inference attacks with increasing diverging properties on tabular, image, and graph datasets to better understand how well an intuitive notion of divergence in properties aligns with observed inference risk. Code for our experiments is available via an anonymized repository [https://github.com/iamgroot42/form\\_est\\_dist\\_risks](https://github.com/iamgroot42/form_est_dist_risks).

##### A. Datasets

We report on experiments using five datasets, summarized in Table I. We construct non-overlapping data splits between the simulated adversary,  $\mathcal{A}$ , and model trainer,  $\mathcal{B}$ . These non-overlapping splits help better capture a realistic scenario where the adversary has access to training data from the distribution  $\mathcal{D}$  but is unlikely to have any training data shared with the victim. Both parties then modify their dataset according to the desired property to emulate a distribution and then sample training datasets from these adjusted distributions to train and evaluate their models. This sampling, along with the disjoint data splits between  $\mathcal{A}$  and  $\mathcal{B}$ , helps ensure the adversary does not inadvertently perform dataset inference by utilizing dataset-specific patterns.

Our experimental datasets were selected to incorporate common benchmarks (Census, CelebA) for comparisons with previous work, new datasets to assess more realistic property inference threats (RSNA Bone Age), as well as applying our definitions beyond ratio-based properties (mean node-degree on ogbn-arxiv, clustering coefficient on Chord). As noted in prior work [6], these target properties for a property inference attack can be either related to or independent of the task and can be either explicit features of the input data or latent features. For instance, attributes varied for Census are feature-based properties since these attributes are directly used as features for the models trained on them. On the other hand, an attribute like the age of a person is unrelated to detecting smiles and is a latent property that is not directly encoded as an input feature

in the training data (but is available for our experiments from provided metadata).

**Census** [20] consists of several categorical and numerical attributes like age, race, education level to predict whether an individual’s annual income exceeds \$50K. We focus on the ratios of whites (race) and females (sex) as properties and use a three-layer feed-forward network as the model architecture.

**RSNA Bone Age** [21] contains X-Ray images of hands, with the task being predicting the patient’s age in months. We convert the task to binary classification based on an age threshold and use a pre-trained DenseNet [22] model for feature extraction, followed by a two-layer network for classification. We focus on the ratios of the females (available as metadata) as properties.

**CelebA** [23] contains face images of celebrities, with multiple images per person. Each image is annotated with forty attributes such as gender, sunglasses, and facial hair. We use two different tasks, smile detection and gender prediction, and train convolutional neural networks from scratch for this dataset. We focus on the ratios of the females (with the smile-detection task) and ratios of old people (with the gender-prediction task) as properties. These attributes in the dataset are defined by a professional labeling company that presumably uses human annotators at some level. We create a network architecture with five convolutional layers and pooling layers, followed by three linear layers.

**ogbn-arxiv** [24] is a directed graph, representing citations between computer science arXiv papers. The task is to predict the subject area categories for unlabeled papers. We infer the mean node-degree property of the graph. We use a four-layer Graph Convolutional Network [25].

**Chord** [26] contains botnets with the Chord [27] topology artificially overlaid on top of background network traffic from CAIDA [28]. The dataset contains multiple graphs, with the task of detecting bot nodes in the graphs. We focus on inferring whether the underlying graphs (onto which we overlay botnets) have average clustering coefficients within a specific range. Following the model architecture proposed in Zhou et al. [26], we implement a variant of the Graph Convolutional architecture.

Dataset	Task	Property	Size		$n_{effective}$	Effectiveness	
			Adversary	Victim		$\ \alpha_0 - \alpha_1\ _{0.75}$	$acc_{(0.4,0.6)}$
Census	Income prediction	Ratio of females	3200	3200	0.8	0.5	74
		Ratio of whites	1800	1800	1.0	0.6	64
CelebA	Smile identification	Ratio of females	22,000	36,000	2.7	0.5	58
	Gender prediction	Ratio of young people	6700	18,800	1.1	0.5	62
RSNA Bone Age	Age prediction	Ratio of females	1800	3600	11.5	0.2	88
ogbn-arxiv Chord	Node classification	Mean node-degree	40,000	97,000	-	-	-
		Average clustering coefficient	135,216	135,523	-	-	-

TABLE I: Descriptions of datasets, along with the effectiveness of inference attacks (best of all Loss Test, Threshold Test, and meta-classifier) while varying ratios of distributions.  $\|\alpha_0 - \alpha_1\|_{0.75}$  is the minimum difference in ratios observed that has at least 75% average accuracy, and  $acc_{(0.4,0.6)}$  is the average distinguishing accuracy when the ratios are (0.4, 0.6).  $n_{effective}$  is the average effective  $n$  value based on our theorem using the maximum distinguishing accuracies across all experiments and pairs of property ratios (without outliers). Size for ogbn-arxiv refers to number of nodes, and the average number of nodes for Chord.

Appendix A provides more details on our experimental setup.

### B. Distinguishing Training Distributions

Current works use arbitrary ratios, like distinguishing between 42% and 59% males [9] while executing property inference attacks. While having one of the ratios corresponding to the estimate of the underlying data distribution is justified, fixing the other arbitrarily makes it hard to understand the adversary’s capabilities—how similar the distributions can get before the adversary can no longer differentiate between them. Additionally, the lack of using the same ratios in experiments while looking at different attributes/properties of the same distribution makes it harder to compare how much information about one property is leaked by models compared to the other. Analyzing such trends can help understand how much of these properties are leaked across different configurations (explicit attribute, latent property) and assess the adversary’s capabilities under different scenarios (black-box access, white-box access).

Since the original ratios for the targeted property may be unbalanced in the dataset (Section II), we fix  $\mathcal{G}_0$  for these experiments such that the resulting distribution is balanced (0.5 ratio) for the chosen attribute for the Census, CelebA, and RSNA Bone Age datasets, setting  $\mathcal{G}_1$  based on varying  $\alpha$  values substituted in Equation 2. For the ogbn-arxiv dataset, we set  $\mathcal{G}_0$  such that the graph has a mean node-degree of 13, and for  $\mathcal{G}_1$ , modify the graph to have a mean-degree  $\alpha$ . For the Chord dataset, we construct  $\mathcal{G}_0$  to have graphs with average clustering-coefficient below 0.0061 and  $\mathcal{G}_1$  to have graphs with average clustering-coefficient above 0.0071. We first try the attacks on a range of distributions as they diverge from a fixed  $\alpha_0$  to evaluate inference risks and understand how well an adversary could distinguish between models trained using different distributions. Later, we vary both distributions simultaneously to understand how similar they can be before the adversary is unable to distinguish between the two (Section IV-C).

**Census.** Figure 4 summarizes the accuracies for all three attack methods across varying proportions of females (left) and whites (right) in the training data. We observe a glaring asymmetry in model performance while varying ratios, along with the lack of

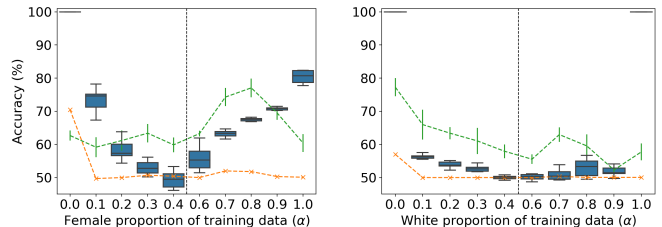


Fig. 4: Classification accuracy for distinguishing between models with different training distributions on the Census dataset for females (left) and whites (right). Orange crosses are for the Loss Test; green with error bars are the Threshold Test; the blue box-plots are the meta-classifiers.

any clear trends showing one attack being consistently better than the others. The Loss Test performs marginally better than random guessing in most cases, while the Threshold Test often outperforms the meta-classifiers.

We observe a clear trend with meta-classifiers while varying  $\alpha$  for the sex attribute: performance improves as distributions diverge ( $\alpha$  further away from 0.5). However, this trend is not symmetric around  $\mathcal{G}_0(\mathcal{D})$ . For example, the adversary performs better on  $\alpha = 0.0$  than  $\alpha = 1.0$ , even though both are equally divergent from  $\mathcal{G}_0(\mathcal{D})$  with respect to female proportion, and have the same upper bound on distinguishing accuracy. This asymmetry also exists for Loss Test and Threshold Test. Even more surprising is the case for race. The meta-classifiers barely do better than random guessing except at the two extremes (0.0, corresponding to no whites at all, and 1.0, corresponding to no non-whites).

*Comparison with previous results.* Ganju et al. [9] applied their meta-classifier method on two properties on this dataset: 38% vs. 65% women (case A), and 0% vs. 87% whites (case B). Both the Loss Test (76.7%) and Threshold Test ( $81.6 \pm 1.3\%$ ) perform well for case B, but do not approach meta-classifier ( $99.4 \pm 0.6\%$ ) performance for case B. For case A, the Threshold Test ( $62.7 \pm 2.0\%$ ) outperforms meta-classifiers

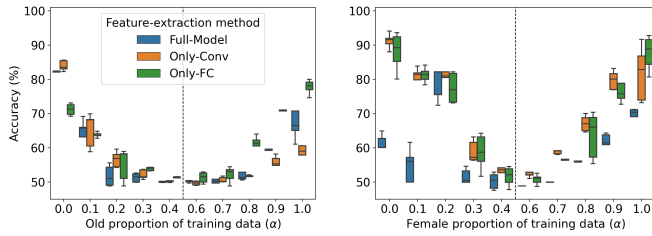


Fig. 5: Classification accuracy for distinguishing between models with different training distributions for the CelebA dataset for old people (left) and females (right). Orange crosses are for the Loss Test; green with error bars are the Threshold Test; the blue box-plots are the meta-classifiers.

( $62.1 \pm 1.7\%$ ), while the Loss Test method fails (50%). Ganju et al. report 97% accuracy for case A and 100% for case B. We were able to closely reproduce these results in the original setting (which consider overlapping data between victim and adversary, and does not ensure changes in ratios do not affect dataset size or class imbalance), but conducted the reported experiments in a more realistic setting where we ensure there is no victim/adversary overlap and maintain the label ratios and same dataset sizes (Appendix A). This leads to huge drops in meta-classifier accuracy, especially in case A (from 97% to 62%), but reduces the risk that the inference is actually based on other differences between the distributions used, not just the inferred property.

**RSNA Bone Age.** The simple Loss Test on this dataset performs quite well, consistently outperforming the Threshold Test and even coming close to meta-classifier performance in some cases. Distinguishing accuracy in this case is quite close to the upper bound derived in Theorem II.1, with  $n_{\text{effective}} \approx 14$ , indicating the adversary’s success in inferring the desired property, despite the effective dataset inferred being significantly smaller than the actual training dataset.

**CelebA.** We include meta-classifier baselines for three variants: using parameters from only linear layers, only convolutional layers, and all layers of the models. We evaluate all three variants on both versions of the CelebA experiment (females and old-people), while varying  $\alpha$ , plotted in Figure 5.

While inferring sex ratios, using parameters only from the linear layers (blue box plots in Figure 5) does not yield satisfactory performance—although it is better than random guessing, it is much worse than when the convolutional layers’ parameters are included. We find that using just the convolutional layers (orange) works as well (sometimes even better) as using all the layers (green). Although including all layers works best when inferring the ratio of old people (left side of Figure 5), we observe that using linear layers performs as good as (sometimes better) than convolutional layers. These trends suggest the likelihood of some layers’ parameters capturing property-related information better than the others. We perform further experiments in Section V that

further support this hypothesis.

We observe trends similar to Census—the meta-classifier exhibit asymmetry, and the Threshold Test comes close to meta-classifier performance (and even out-performs in some cases, like 0.0 and 0.2 ratios for old people) in many cases, while the Loss Test performs only slightly better (worse, at times) than random. Worse-than-random accuracy may occur if the adversary’s dataset is not representative of the data used by the victim.

**ogbn-arxiv.** We vary  $\alpha$  in the range [9, 17] at intervals of one, producing test datasets by pruning either high or low-degree nodes from the original graph to achieve a desired  $\alpha$ . Like the other datasets, meta-classifier performance increases as the distributions diverge, albeit with much smaller drops. The meta-classifier is highly successful at differentiating between the two distributions even when the difference in mean node-degrees is just one (Figure 7), achieving  $\geq 90\%$  accuracy in all cases. Both Loss Test and Threshold Test fail on this dataset.

We also trained a regression variant of the meta-classifier to predict  $\alpha$  directly. The resulting meta-classifier performs quite well, achieving a mean-squared error (MSE) loss of  $0.393 \pm 0.36$ . It generalizes well to unseen distributions, achieving an average MSE loss of 0.076 for  $\alpha=12.5$  and 13.5. A property inference adversary can thus be strong enough to directly predict the actual average node degree of the training dataset.

**Chord.** For the case where both victim and adversary’s training datasets are sampled from the same pool of data, the adversary has near-perfect distinguishing accuracy, even when training the meta-classifier with ten models (and testing on 1000). However, the adversary cannot achieve the same level of performance in the absence of data overlap. Using the Loss Test yields an accuracy of 63.18%, while the Threshold Test and meta-classifier struggle to perform better than random ( $\sim 51\%$ ). This disparity in performance further justifies our experimental design choice to consider non-overlapping data splits—evaluating property inference attacks on models trained from the same dataset pool seems effective, but it is really just learning some unrelated property that distinguishes between datasets. Additionally, the gap in meta-classifier performance and the simple Loss Test suggests there might exist better methods that could infer properties even under the non-overlapping scenario.

**Overall Trends.** Although we observe an increase in performance across all our experiments as the distributions diverge from  $\mathcal{G}_0(\mathcal{D})$ , these trends are not symmetric. In all of the datasets above, one side of the graph has visibly better performance than the other, despite being symmetric in the upper bounds on distinguishing accuracies. This suggests a bias in the learning algorithm used to train these models, or perhaps the meta-classifier’s capability to extract training datasets effectively. Additionally, the lack of any clear ranking of the three attacks shows why it is necessary to include simple baselines when evaluating property inference risk. In fact, the inexpensive Threshold Test does better than meta-classifiers

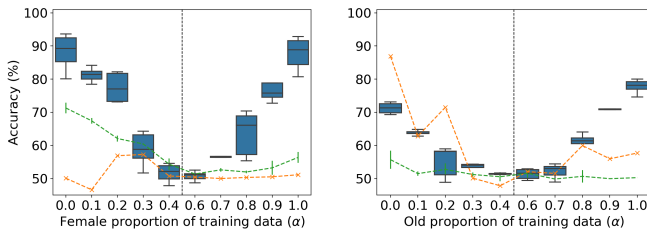


Fig. 6: Classification accuracy for distinguishing between models with different training distributions for the CelebA when varying the ratio of females (left) and old people (right).

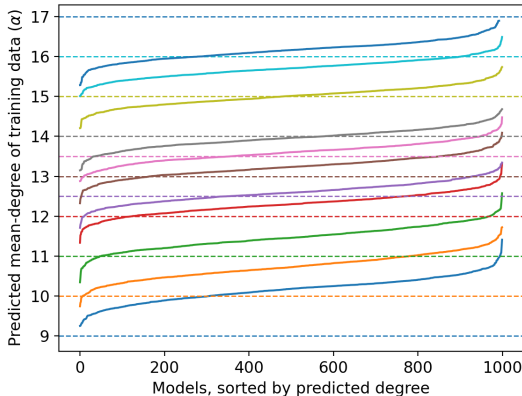


Fig. 7: Performance on unseen models on ogbn-arxiv dataset for direct  $\alpha$  prediction via regression. Each color represents the true degree (dashed lines) of the models being tested.

$\sim 30\%$  of the time.

Given an observed accuracy  $a$  for two ratios  $\alpha_0, \alpha_1$ , the effective dataset size can be computed as:

$$n_{\text{effective}} = \frac{\log(1 - (2a - 1)^2)}{\log(\max(\frac{\min(\alpha_0, \alpha_1)}{\max(\alpha_0, \alpha_1)}, \frac{1 - \max(\alpha_0, \alpha_1)}{1 - \min(\alpha_0, \alpha_1)}))}. \quad (6)$$

We also observe that  $n_{\text{effective}}$  (Theorem II.1) values are far from the dataset sizes in nearly all cases. This suggests how the models themselves effectively leak only a small fraction of their training data, and that even values less than one are sufficient for the adversary to launch successful property inference attacks. We observe this value to be highest for RSNA Bone Age on an average (Table I). Similar to asymmetric performance trends, we observe a sharp increase in  $n_{\text{effective}}$  values as the distributions diverge from each other. Cases like the extremes of Census (race) reach 100% accuracies and thus, correspond to the trained model leaking all of the dataset’s privacy with regards to the property under focus.

### C. Varying Distribution Similarity

An adversary may not necessarily be interested in distinguishing between the balanced case ( $\alpha = 0.5$ ) and other ratios. For instance, health datasets for specific ailments may have a higher underlying prevalence in females, and the adversary may be interested in differentiating between two particular

ratios of females, like 0.3 and 0.4. We thus experiment with the case where both distributions are varied:  $\mathcal{G}_0(\mathcal{D})$  and  $\mathcal{G}_1(\mathcal{D})$  with corresponding ratios  $\alpha_0$  and  $\alpha_1$  respectively. Observing performance trends as the difference in ratios increases helps us understand how much of a threat property inference may pose as the similarity of the distributions varies. For instance, according to Theorem II.1, (0.1, 0.2) and (0.5, 0.6) for  $n = 2$  (considering CelebA) have an upper bound on distinguishing accuracy of  $\sim 73\%$  and  $\sim 78\%$  respectively, despite having the same difference in ratios, while experimental results for these ratios on CelebA exhibit opposite trends: 60% and 55% for females, and 53% and 52% for old people, for the ratios (0.1, 0.2) and (0.5, 0.6).

**Observations.** Figure 8 shows distinguishing accuracies between models (in the form of heatmaps) trained on distributions  $\mathcal{G}_0(\mathcal{D})$ ,  $\mathcal{G}_1(\mathcal{D})$  while varying corresponding  $\alpha_0$  and  $\alpha_1$  simultaneously, for ratios of females on Census and CelebA. We also compute  $n_{\text{effective}}$  for each of these cases and visualize them in the same heatmaps. For instance,  $(\alpha_0, \alpha_1) = (0.2, 0.9)$  in the upper-right triangle correspond to meta-classifier performance (70%), while  $(\alpha_0, \alpha_1) = (0.9, 0.2)$  in the lower-left triangle corresponds to  $n_{\text{effective}}$  for that configuration and accuracy (0.12). Heatmaps for the other cases/datasets are available in Appendix D. Entries along a given diagonal have the same value of  $|\alpha_0 - \alpha_1|$ . We observe accuracy values to be roughly in the same range along diagonals. The variance in performance across runs is relatively high for similar distributions (small  $|\alpha_0 - \alpha_1|$ ) and decreases as the distributions become more and more different. Similar to results for the case where one distribution is fixed (Section IV-B), we observe asymmetry in performance.

However, there are some peculiar trends in each of the datasets. For example, on the Census dataset, the adversary has notably high accuracy in differentiating between distributions when one is without any females ( $\alpha_i = 0$ ) or males ( $\alpha_i = 1$ ), regardless of the actual proportion of females in the data. This suggests that detecting the mere presence or absence of members with a particular attribute is significantly easier than trying to deduce the exact ratio of members with that attribute. Similarly, a difference in ratios of  $\geq 0.3$  on RSNA Bone Age or two in mean node-degree both yield at least 90% accuracy for all cases using meta-classifiers. There are a few deviations in performance trends for some  $(\alpha_0, \alpha_1)$  combinations. We also observe that along any given diagonal, performance increases as either of  $\alpha_0, \alpha_1$  increases or decreases, which is in line with the derived upper bound (Theorem II.1).

Unlike Census, performance on CelebA at the extremes (no males or females when inferring sex ratios, and no young or old people when inferring old ratios) are far from perfect. This may be because features like race and gender in Census are directly used for model training, and thus their presence or absence would directly impact model parameters. However, in this case, the complicated feature extractor may not embed these latent (and inherently ambiguous) properties explicitly.

For CelebA (sex) and Census (sex), we observe that  $n_{\text{effective}}$



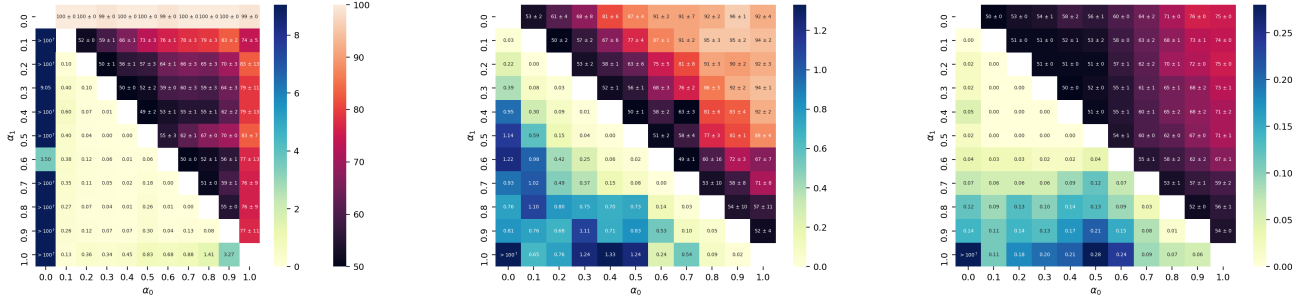


Fig. 8: Classification accuracies (top-right triangle) and  $n_{\text{effective}}$  values (bottom-left triangles) for distinguishing between training distributions  $\mathcal{G}_0(\mathcal{D})$  with ratio  $\alpha_0$  and  $\mathcal{G}_1(\mathcal{D})$  with ratio  $\alpha_1$ , using meta-classifiers on Census (left) and CelebA (middle), and Threshold Test on CelebA (right).  $n_{\text{effective}} > 100^\dagger$  corresponds to cases where adversary can distinguish nearly perfectly (within the error margin of the experiment, approaching the upper bound given by the size of the training dataset).

is less very low ( $< 1$ ) in most cases. These extremely small values demonstrate how little information is necessary for a somewhat effective property inference attacks, and how close the distributions can be for the attack to still perform at some level of accuracy. Unlike trends in accuracies, patterns in  $n_{\text{effective}}$  values do not exhibit smooth transitions even though some trends do emerge when moving across diagonals (varying  $|\alpha_0 - \alpha_1|$ ).

*White-box vs. Black-box.* There are many instances where either of the two simple black-box tests perform exceptionally well—even better than meta-classifier. For instance, Threshold Test on Census (race) and Loss Test on CelebA (old) outperform the meta-classifiers for nearly all of pairs of ratios. These observations further support the approach of using more direct attacks like Loss Test and Threshold Test before training expensive meta-classifiers, especially since there is no clear ordering of these attacks across datasets and ratios. However, on average, the meta-classifiers to outperform both Loss Test and Threshold Test. Thus, for the remainder of the paper we focus on meta-classifier attacks.

## V. IDENTIFYING IMPORTANT MODEL LAYERS

Meta-classifier attacks are expensive and deciphering what meta-classifiers learn is challenging—this is especially true with Permutation-Invariant Networks that apply complex operations on the actual model parameters. Identifying critical parameters can both improve understanding and lower resource requirements, using just a fraction of the model’s parameters for meta-classifiers, leading to comparable performance with fewer models and lower training costs.

Here, we propose a simple test to help the adversary rank and identify the most relevant layers for distinguishing between the given distributions (Section V-A), and show that training meta-classifiers on just the important layers can substantially reduce the cost of the attack without compromising effectiveness (Section V-B).

### A. Identifying Useful Layers

Let  $j$  be some layer of the model for which the adversary wishes to gauge property-inference potential. We optimize query point  $\hat{x}$  to maximize the difference in the total number of activations for layer  $j$  between models trained on datasets from the two distributions:

$$M_j(x) = \sum_i \mathbb{I}[(M[:j](x))_i > 0]$$

$$\hat{x} = \arg \max_x \left| \sum_{i:y_i=0} M_j^i(x) - \sum_{i:y_i=1} M_j^i(x) \right|, \quad (7)$$

where  $M[:j](x)$  refers to the activations after layer  $j$  of model  $M$  on input  $x$ . The adversary can use a set of test points to select the point that maximizes the above constraint or use gradient ascent to generate such a query point directly. Then, similar to the process for Threshold Test (Equation 5), the adversary finds a threshold on the number of activations to maximize distinguishing accuracy. By iterating through all layers and computing the corresponding accuracies, the adversary can create a ranking of layers to estimate how much information these layers can potentially leak. This process is computationally much cheaper than running a meta-classifier experiment for all layers. The adversary can use as few as 20 models and even make do without any test points (in cases where it can generate data, like images) to generate this ranking.

Once it has ranked all of them, the adversary can pick the most informative layers (even one suffices in some cases) to train meta-classifiers. Since the resulting meta-classifier has fewer parameters (as it computes over fewer model layers), the adversary can use significantly fewer models than using all the layers’ parameters, without having a significant impact on distinguishing accuracy.

### B. Results

To understand how well the layer-identification process correlates with meta-classifier performance, we also perform experiments where each layer’s parameters are used one at a time to train the meta-classifier. We run the layer-identification

Dataset	Layer						
	1	2	3	4	5	6	7
CelebA (female)	<b>89.2</b>	76.7	75.8	74.2	70.0	66.7	63.3
CelebA (old)	64.2	60	60	68.3	<b>73.3</b>	70	66.7
Census (female)	<b>62.0</b>	58.0	56.4	-	-	-	-
Census (white)	<b>81.7</b>	75.0	63.3	-	-	-	-
RSNA Bone Age	<b>65.0</b>	64.0	-	-	-	-	-
ogbn-arxiv	93.3	95.0	<b>98.3</b>	-	-	-	-
Chord	69.4	60.0	64.0	64.8	57.2	50.2	-

TABLE II: Maximum accuracy using layer-identification method. Since the last layer in all of these models is used for classification with a Softmax/Sigmoid activation, the process in Equation 7 cannot be applied to the last layer.

process, as described in Eq 7, for all layers across datasets. As visible in Table II, for most cases the layers closest to the inputs are identified as most useful. These accuracies for CelebA align with observations from previous experiments (Section IV-B) as well—for distinguishing sex ratios, the convolutional layers (until layer 5) seem to be more useful; for age, the fully-connected layers appear to be most useful. Layers of machine-learning models closer to the input are commonly associated with learning generic patterns, and later layers more abstract ones along with invariance to the given task [29]. Thus, the position of layers identified to be most useful is telling of how close the target property is to the input space or task.

Using these observations, we train meta-classifiers while using parameters only from some of the layers selected on the ranking we obtain via layer-identification experiments. We observe a clear advantage of doing so across all datasets, with minimal decreases in accuracy. For instance, using just the first layer produces an accuracy meta-classifier with only 20 training models on RSNA Bone Age (orange boxes in leftmost graph in Figure 9) performs much better than using parameters from all of the layers, which approaches the accuracy of the one-layer meta-classifier much slower.

For datasets like Census, all the layers seem to equally useful while for RSNA Bone Age, only the first layers’ parameters are useful. When using the first layer’s parameters, the adversary can achieve an average of 75% accuracy with as few as 20 models, compared to 54% when using the entire model. In fact, the first layer is identified as most useful and using any other layer leads to near-random performance. Additionally, for larger models like those for CelebA, the adversary can pick more than one layer—using as few as three layers of the model can help lower computational resources. As observed in ablation experiments with convolutional and linear layers for CelebA (old people), using just the last three layers (of which two the layer-identification process identifies), the adversary can train its meta-classifiers while using significantly fewer models. For instance, when using 100 models to train the meta-classifier, using just the fully-connected layers gives a 4% absolute improvement in accuracy, along with 0.5% reduction in standard deviation across experiments.

*Graph Datasets.* The layer-identification process does not work on the graph datasets. It incorrectly predicts the third layer

as most useful for ogbn-arxiv, whereas actual performance with that layer’s parameters leads to a significant performance drop. This behavior can be explained by the inherent difference in data-structure. Intermediate activations for nodes can have complicated interactions with neighboring nodes, leading to the detection method’s instability when analyzing activation values. These shortcomings on graph datasets is something that we wish to further investigate in future work. Nonetheless, the fact the first two layers are useful for both ogbn-arxiv and Chord may serve as a rule-of-thumb for graph-based property inference attacks.

## VI. CONCLUSIONS

We propose a general definition for property inference attacks, focusing on distributions instead of datasets. Our definition supports arbitrary properties like the mean node-degree of a graph, which we demonstrate an adversary can successfully infer even with when the victim’s and adversary’s data do not overlap. A systematic approach to evaluating such attacks reveals how intuition may not necessarily align with actual performance—seemingly similar pairs of distributions can have starkly different attack success rates, and simple attacks can outperform computationally expensive meta-classifier at times. We expect there is room for improving attacks that do not rely on meta-classifiers, and studying the performance of such attacks will provide more valuable insights into how well properties can be inferred and under what circumstances. The ability to identify and use only a part of the models’ parameters suggests there is scope to design attacks. The observed asymmetry across several datasets while inferring ratios indicates bias amplification or imperfections in datasets.

Our theorem provides a way to estimate the effective size  $n_{effective}$  of the reconstructed dataset that is comparable to the property inference attack, so that they may allocate and utilize their resources accordingly. Small  $n_{effective}$  values are indicative of distributions which are relatively easy for adversaries, even under extreme cases of recovering a fraction of a single training datum. Although our theorem only applies to binary membership properties, there is scope to develop such bounds for any two generic distributions using the same framework.

There could exist trade-offs between accuracy, robustness, fairness, interpretability, and vulnerability to property inference attacks. For instance, a model that is fair with regards to

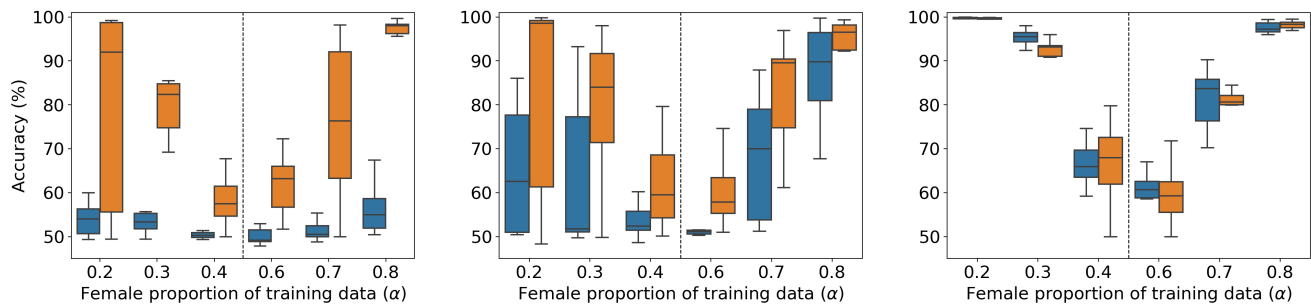


Fig. 9: Classification accuracy for distinguishing between models with different training distributions on the RSNA Bone Age dataset. Left to right: meta-classifiers trained using 10, 40, and 1600 (original experiment) models, respectively. Orange box plots correspond to using parameters only from the first layer, while blue box plots correspond to using all (three) layers' parameters.

its predictions for males/females would probably be immune to property-inference attacks on this attribute. Expanding the proposed framework to incorporate these trade-offs and include scenarios like poisoning is part of our ongoing work.

We hope our contributions (especially observations on Census-race and Chord) motivate researchers in the field to consider more realistic and controlled configurations; as we demonstrate, there can be a massive difference in results if the underlying experimental structure is not designed carefully. The ability of our framework to capture properties beyond ratios of binary functions, along with results on properties like the mean node-degree on graphs, should encourage researchers to explore more creative and sensitive properties.

#### Acknowledgements

The authors thank Justin Chen for contributing to some of the experiments in this paper, along with Xiao Zhang, Bargav Jayaraman, and Ambar Pal for helpful feedback on the paper including a detailed reading of our proof. This work was partially supported by grants from the National Science Foundation (#1717950 and #1915813), and funding from Lockheed Martin Corporation.

#### REFERENCES

- [1] R. Shokri, M. Stronati, C. Song, and V. Shmatikov, "Membership Inference Attacks against Machine Learning Models," in *IEEE Symposium on Security and Privacy*, 2017.
- [2] G. Ateniese, L. V. Mancini, A. Spognardi, A. Villani, D. Vitali, and G. Felici, "Hacking Smart Machines with Smarter Ones: How to Extract Meaningful Data from Machine Learning Classifiers," *International Journal of Security and Networks*, vol. 10, no. 3, pp. 137–150, 2015.
- [3] M. Iliofotou, H.-c. Kim, M. Faloutsos, M. Mitzenmacher, P. Pappu, and G. Varghese, "Graph-based P2P traffic classification at the Internet backbone," in *IEEE INFOCOM Workshops*, 2009.
- [4] D. Gopinath, H. Converse, C. Pasareanu, and A. Taly, "Property Inference for Deep Neural Networks," in *34th IEEE/ACM International Conference on Automated Software Engineering*, 2019.
- [5] M. Jedorova, C. Kaul, C. Mayor, A. Q. O'Neil, A. Weir, R. Murray-Smith, and S. A. Tsafaris, "Survey: Leakage and Privacy at Inference Time," *arXiv preprint arXiv:2107.01614*, 2021.
- [6] W. Zhang, S. Tople, and O. Ohrimenko, "Leakage of dataset properties in multi-party machine learning," in *30th USENIX Security Symposium*, 2021.
- [7] D. Kifer and A. Machanavajjhala, "Pufferfish: A Framework for Mathematical Privacy Definitions," *ACM Transactions on Database Systems (TODS)*, 2014.
- [8] M. Chase, E. Ghosh, and S. Mahloujifar, "Property Inference from Poisoning," *arXiv:2101.11073*, 2021.
- [9] K. Ganju, Q. Wang, W. Yang, C. A. Gunter, and N. Borisov, "Property Inference Attacks on Fully Connected Neural Networks using Permutation Invariant Representations," in *ACM Conference on Computer and Communications Security*, 2018.
- [10] X. Xu, Q. Wang, H. Li, N. Borisov, C. A. Gunter, and B. Li, "Detecting AI Trojans Using Meta Neural Analysis," in *IEEE Symposium on Security and Privacy*, 2021.
- [11] J. Hestness, S. Narang, N. Ardalani, G. Diamos, H. Jun, H. Kianinejad, M. Patwary, M. Ali, Y. Yang, and Y. Zhou, "Deep Learning Scaling is Predictable, Empirically," *arXiv preprint arXiv:1712.00409*, 2017.
- [12] M. Hay, C. Li, G. Miklau, and D. Jensen, "Accurate Estimation of the Degree Distribution of Private Networks," in *Ninth IEEE International Conference on Data Mining*, 2009.
- [13] M. Fredrikson, E. Lantz, S. Jha, S. Lin, D. Page, and T. Ristenpart, "Privacy in Pharmacogenetics: An End-to-End Case Study of Personalized Warfarin Dosing," in *23rd USENIX Security Symposium*, 2014.
- [14] P. Maini, M. Yaghini, and N. Papernot, "Dataset Inference: Ownership Resolution in Machine Learning," in *International Conference on Learning Representations*, 2021.
- [15] B. Wang and N. Z. Gong, "Stealing Hyperparameters in Machine Learning," in *IEEE Symposium on Security and Privacy*, 2018.
- [16] N. Carlini, F. Tramèr, E. Wallace, M. Jagielski, A. Herbert-Voss, K. Lee, A. Roberts, T. Brown, D. Song, U. Erlingsson, A. Oprea, and C. Raffel, "Extracting training data from large language models," in *USENIX Security Symposium*, 2021.
- [17] L. Lyu and C. Chen, "A Novel Attribute Reconstruction Attack in Federated Learning," *arXiv preprint arXiv:1712.00409*, 2021.
- [18] S. Yeom, I. Giacomelli, M. Fredrikson, and S. Jha, "Privacy Risk in Machine Learning: Analyzing the Connection to Overfitting," in *31st IEEE Computer Security Foundations Symposium*, 2018.
- [19] M. Zaheer, S. Kottur, S. Ravanbakhsh, B. Poczos, R. R. Salakhutdinov, and A. J. Smola, "Deep Sets," *Advances in Neural Information Processing Systems*, 2017.
- [20] S. D. Bay, D. Kibler, M. J. Pazzani, and P. Smyth, "The UCI KDD Archive of Large Data Sets for Data Mining Research and Experimentation," *ACM SIGKDD Explorations Newsletter*, vol. 2, no. 2, pp. 81–85, 2000.
- [21] S. S. Halabi, L. M. Prevedello, J. Kalpathy-Cramer, A. B. Mamonov, A. Bilbily, M. Cicero, I. Pan, L. A. Pereira, R. T. Sousa, N. Abdala et al., "The RSNA Pediatric Bone Age Machine Learning Challenge," *Radiology*, vol. 290, no. 2, pp. 498–503, 2019.
- [22] G. Huang, Z. Liu, L. Van Der Maaten, and K. Q. Weinberger, "Densely Connected Convolutional Networks," in *IEEE/CVF Conference on Computer Vision and Pattern Recognition*, 2017.
- [23] Z. Liu, P. Luo, X. Wang, and X. Tang, "Large-scale CelebFaces Attributes (CelebA) Dataset," 2018.

- [24] K. Wang, Z. Shen, C. Huang, C.-H. Wu, Y. Dong, and A. Kanakia, "Microsoft Academic Graph: When experts are not enough," *Quantitative Science Studies*, vol. 1, no. 1, pp. 396–413, 2020.
- [25] T. N. Kipf and M. Welling, "Semi-supervised classification with graph convolutional networks," in *International Conference on Learning Representations*, 2017.
- [26] J. Zhou, A. M. Xu, Zhiying amd Rush, and M. Yu, "Automating Botnet Detection with Graph Neural Networks," *AutoML for Networking and Systems Workshop of MLSys 2020 Conference*, 2020.
- [27] I. Stoica, R. Morris, D. Liben-Nowell, D. R. Karger, M. F. Kaashoek, F. Dabek, and H. Balakrishnan, "Chord: a scalable peer-to-peer lookup protocol for Internet applications," *IEEE/ACM Transactions on Networking*, vol. 11, no. 1, pp. 17–32, 2003.
- [28] Center for Applied Internet Data Analysis, "The CAIDA UCSD Anonymized Internet Traces," [https://www.caida.org/data/passive/passive\\_dataset.xml](https://www.caida.org/data/passive/passive_dataset.xml), 2018.
- [29] V. Papyan, X. Y. Han, and D. L. Donoho, "Prevalence of neural collapse during the terminal phase of deep learning training," *Proceedings of the National Academy of Sciences*, vol. 117, no. 40, 2020.
- [30] Mathematics State Exchange User 'user13888', "What is the relationship of  $\mathcal{L}_1$  (total variation) distance to hypothesis testing?" Mathematics Stack Exchange, <https://math.stackexchange.com/q/72730>, 2011.
- [31] H. Jain, "Applications of Pinsker's inequality," Harvard Course Notes, <http://people.seas.harvard.edu/~madhusudan/courses/Spring2016/scribe/lect07.pdf>.
- [32] A. B. Tsybakov, "Introduction to Nonparametric Estimation," 2009.

### A. Attack Details

We perform each experiment ten times and report mean values with standard deviation in all of our experiments. Since the Loss Test uses a fixed test set per experiment, its results show no variation. The model trainer produces 1000 models per distribution using its split of data. These models serve as the evaluation set. Thus, any particular experiment distinguishing between two distributions trains 2000 models. The adversary trains 100 models per distribution on its data split for the Threshold Test and meta-classifier experiments.

**Loss Test.** The adversary uses its test data to sample the two test sets  $S_0, S_1$ . Since we use the same test data in evaluations, we turn off sampling while generating data with desired properties (see above) for this setting.

**Threshold Loss.** The adversary uses a sample size of 100 models (50 per distribution).

**Meta-Classifer.** We used Permutation Invariant Networks as our meta-classifier architecture [9]. The adversary randomly samples 1600 models from its pool to train the meta-classifier. Following experimental designs from prior works, we were able to achieve the accuracies that the authors reported. However, we notice that, for some cases, using our experimental design leads to significant performance drops. Steps like ensuring no overlap in victim/adversary training data, randomly sampled datasets for  $\mathcal{G}_0(\mathcal{D})$ ,  $\mathcal{G}_1(\mathcal{D})$ , ensuring the same dataset size, introduce stochasticity that makes it for a meta-classifier to perform as well. Thus, these steps help emulate a more realistic scenario but adversely impact meta-classifier in some cases.

### B. Proof of Theorem

Assume the adversary can fully recover a dataset  $S$  (of size  $n$ ) from some model  $M$  trained on it. Assume  $\psi(\cdot)$  is an estimator for testing the hypothesis, i.e.  $\psi(S) = b_{\in\{0,1\}}$  means that  $S$  comes from  $\mathcal{G}_b(\mathcal{D})$ . Assuming an equal likelihood of the chosen dataset  $S$  being from either distributions, we have:

$$\begin{aligned} \text{Error} &= \frac{1}{2}(\Pr_{S \leftarrow \mathcal{G}_0(\mathcal{D})^n}[\psi(S) = 1] + \Pr_{S \leftarrow \mathcal{G}_1(\mathcal{D})^n}[\psi(S) = 0]) \\ &= \frac{1}{2}(\text{Type I Error} + \text{Type II Error}). \end{aligned}$$

Combining with the result from [30]:

$$\text{Error} \geq \frac{1}{2} - \frac{1}{2}\delta(\mathcal{G}_0(\mathcal{D})^n, \mathcal{G}_1(\mathcal{D})^n) \quad (8)$$

$$\Rightarrow \text{Accuracy} \leq \frac{1}{2} + \frac{1}{2}\delta(\mathcal{G}_0(\mathcal{D})^n, \mathcal{G}_1(\mathcal{D})^n), \quad (9)$$

where  $\delta(\cdot)$  is the total variation distance between two probability measures. Thus, the maximum accuracy while differentiating between datasets sampled from either distribution is bounded by the total variation distance between them.

Let  $\rho_b(x)$  be the generative probability density function for some sample  $x$  drawn from  $\mathcal{G}_b(\mathcal{D})$ , for  $b \in \{0, 1\}$ . This density function can then be broken down into a multinomial distribution and priors as:

$$\rho_b(x) = (1 - \alpha_b)p_b(\mathbf{x}|0) + \alpha_b p_b(\mathbf{x}|1), \quad (10)$$

where  $\alpha_b$  is the prior for  $p(1)$  corresponding to  $\mathcal{G}_b(\mathcal{D})$ , and  $\rho_b(x|1)$  is the associated conditional generative probability density function. Note that  $p_0(\mathbf{x}|0) = p_1(\mathbf{x}|0)$  and  $p_0(\mathbf{x}|1) = p_1(\mathbf{x}|1)$ , since they both come from the underlying distribution  $\mathcal{D}$ . Without loss of generality, let  $\alpha_0 > \alpha_1$  (we omit the case of same ratios, since that is trivially indistinguishable). Then:

$$\begin{aligned} \alpha_1 \rho_0(x) - \alpha_0 \rho_1(x) &= \alpha_1((1 - \alpha_0)p_0(\mathbf{x}|0) + \alpha_0 p_0(\mathbf{x}|1)) - \alpha_0((1 - \alpha_1)p_1(\mathbf{x}|0) + \alpha_1 p_1(\mathbf{x}|1)) \\ &= \alpha_1 p_0(\mathbf{x}|0) - \alpha_1 \alpha_0 p_0(\mathbf{x}|0) + \alpha_0 \alpha_1 p_0(\mathbf{x}|1) - (\alpha_0 p_1(\mathbf{x}|0) - \alpha_0 \alpha_1 p_1(\mathbf{x}|0) + \alpha_1 \alpha_0 p_1(\mathbf{x}|1)) \\ &= (\alpha_1 - \alpha_0)p_0(\mathbf{x}|0) \\ &\leq 0 \\ \Rightarrow \frac{\rho_0(x)}{\rho_1(x)} &\leq \frac{\alpha_0}{\alpha_1} \end{aligned} \quad (11)$$

Using this inequality, the relative entropy (KL divergence) from  $\mathcal{G}_1(\mathcal{D})$  to  $\mathcal{G}_0(\mathcal{D})$  can be written as:

$$D_{KL}(\mathcal{G}_0(\mathcal{D})\|\mathcal{G}_1(\mathcal{D})) = \int \rho_0(x) \log\left(\frac{\rho_0(x)}{\rho_1(x)}\right) dx \quad (12)$$

$$\leq \int \rho_0(x) \log\left(\frac{\alpha_0}{\alpha_1}\right) dx \quad (13)$$

$$= \log\left(\frac{\alpha_0}{\alpha_1}\right) \int \rho_0(x) dx \quad (14)$$

$$= \log\left(\frac{\alpha_0}{\alpha_1}\right) \quad (15)$$

Since the function  $f$  is binary, a prior of  $\alpha_b$  for  $p(f(x) = 1)$  implies a prior of  $(1 - \alpha_b)$  for  $p(f(x) = 0)$ . Utilizing this symmetry, we can similarly upper-bound  $D_{KL}(\mathcal{G}_1(\mathcal{D})\|\mathcal{G}_0(\mathcal{D}))$  with  $\log\left(\frac{1-\alpha_1}{1-\alpha_0}\right)$ . Removing the  $\alpha_0 \geq \alpha_1$  assumption and replacing with the max/min of these two appropriately, we get:

$$D_{KL}(\mathcal{G}_0(\mathcal{D})\|\mathcal{G}_1(\mathcal{D})) \leq \log\left(\frac{\max(\alpha_0, \alpha_1)}{\min(\alpha_0, \alpha_1)}\right) \quad (16)$$

$$D_{KL}(\mathcal{G}_1(\mathcal{D})\|\mathcal{G}_0(\mathcal{D})) \leq \log\left(\frac{1 - \min(\alpha_0, \alpha_1)}{1 - \max(\alpha_0, \alpha_1)}\right)$$

From [31], we know that:

$$D_{KL}(\mathcal{G}_0(\mathcal{D})^n\|\mathcal{G}_1(\mathcal{D})^n) = nD_{KL}(\mathcal{G}_0(\mathcal{D})\|\mathcal{G}_1(\mathcal{D})) \quad (17)$$

Thus, when using a dataset  $S$  of size  $|S| = n$ , the equivalent KL-divergence can be bounded by:

$$D_{KL}(\mathcal{G}_0(\mathcal{D})^n\|\mathcal{G}_1(\mathcal{D})^n) \leq n \log\left(\frac{\max(\alpha_0, \alpha_1)}{\min(\alpha_0, \alpha_1)}\right) \quad (18)$$

$$D_{KL}(\mathcal{G}_1(\mathcal{D})^n\|\mathcal{G}_0(\mathcal{D})^n) \leq n \log\left(\frac{1 - \min(\alpha_0, \alpha_1)}{1 - \max(\alpha_0, \alpha_1)}\right)$$

Using the relation between total variation distance and KL-divergence [32], we know:

$$\delta(\mathcal{G}_0(\mathcal{D})^n, \mathcal{G}_1(\mathcal{D})^n) \leq \sqrt{1 - e^{-D_{KL}(\mathcal{G}_0(\mathcal{D})^n\|\mathcal{G}_1(\mathcal{D})^n)}} \quad (19)$$

$$= \sqrt{1 - e^{-n \log\left(\frac{\max(\alpha_0, \alpha_1)}{\min(\alpha_0, \alpha_1)}\right)}} \quad (20)$$

$$= \sqrt{1 - \left(\frac{\min(\alpha_0, \alpha_1)}{\max(\alpha_0, \alpha_1)}\right)^n} \quad (21)$$

Similarly, using  $D_{KL}(\mathcal{G}_1(\mathcal{D})\|\mathcal{G}_0(\mathcal{D}))$  in the inequality above we get:

$$\delta(\mathcal{G}_0(\mathcal{D})^n, \mathcal{G}_1(\mathcal{D})^n) \leq \sqrt{1 - e^{-D_{KL}(\mathcal{G}_1(\mathcal{D})^n\|\mathcal{G}_0(\mathcal{D})^n)}} \quad (22)$$

$$= \sqrt{1 - e^{-n \log\left(\frac{1 - \min(\alpha_0, \alpha_1)}{1 - \max(\alpha_0, \alpha_1)}\right)}} \quad (23)$$

$$= \sqrt{1 - \left(\frac{1 - \max(\alpha_0, \alpha_1)}{1 - \min(\alpha_0, \alpha_1)}\right)^n} \quad (24)$$

Since the function  $f()$  is boolean, an adversary can choose to focus on a property value of 0 or 1, and infer the ratio of one using the other. Thus, any two ratios  $(\alpha_0, \alpha_1)$  can be alternatively seen as  $(1 - \alpha_0, 1 - \alpha_1)$ . Combining the two inequalities above and plugging them back in (9), we get:

$$\text{Accuracy} \leq \frac{1}{2} + \frac{\min\left\{\sqrt{1 - \left(\frac{\min(\alpha_0, \alpha_1)}{\max(\alpha_0, \alpha_1)}\right)^n}, \sqrt{1 - \left(\frac{1 - \max(\alpha_0, \alpha_1)}{1 - \min(\alpha_0, \alpha_1)}\right)^n}\right\}}{2} \quad (25)$$

Note that the proof of this bound hinges on both the distributions originating from the same underlying distribution  $\mathcal{D}$ , which is why we use  $\mathcal{G}_0(\mathcal{D})$ ,  $\mathcal{G}_1(\mathcal{D})$  instead of some arbitrarily defined distributions  $\mathcal{D}_0$ ,  $\mathcal{D}_1$ .

### C. Identifying Useful Layers

The adversary uses a small sample of 20 models for layer-identification experiments. For the numbers reported in Table II, the adversary samples data from its local test set to maximize Equation 7. Distinguishing accuracies reported in this table are on the adversary’s models since it uses this ranking of layers to train a meta-classifier for its attack on the victim’s model(s).

We hypothesize that excluding the last layer does not lead to a significant performance drop—intuitively, layers closer to the output will capture invariance for the given task and are thus less likely to contain any helpful information that prior layers would not already capture. Results from layer-wise meta-classifier experiments confirm how the last layer’s parameters are rarely useful for property inference.

### D. Additional Figures

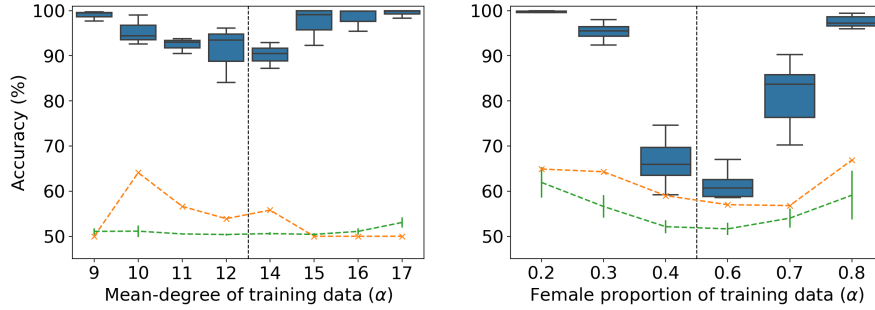


Fig. 10: Classification accuracy for distinguishing between models with different training distributions on the ogbn-arxiv (left) and RSNA Bone Age (right) datasets. Orange crosses are for the Loss Test; green with error bars are the Threshold Test; the blue box-plots are the meta-classifiers.

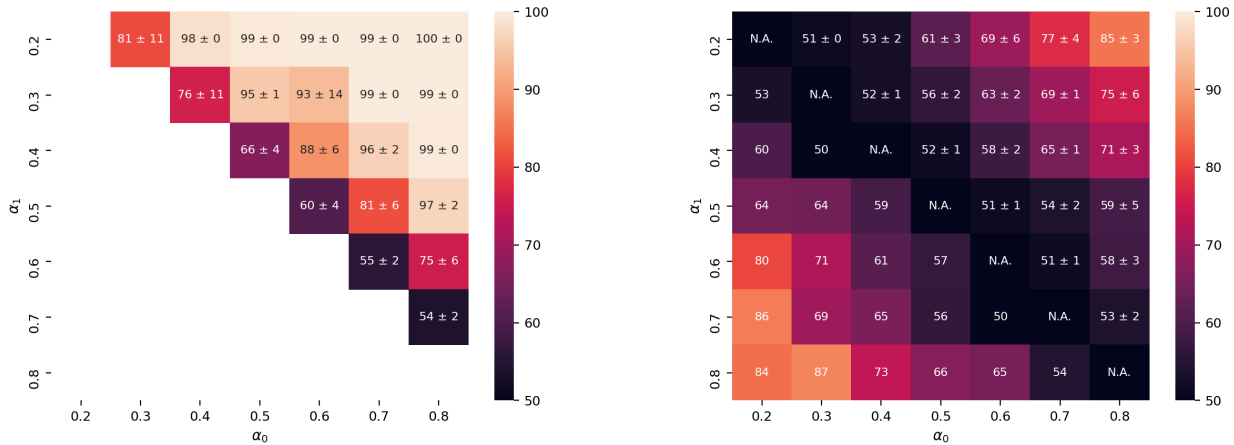


Fig. 11: Classification accuracy using meta-classifiers (left), Loss Test (right, lower triangle), and Threshold Test (right, upper triangle), for distinguishing between models with training distributions  $\mathcal{G}_0(\mathcal{D})$  with ratio  $\alpha_0$  and  $\mathcal{G}_1(\mathcal{D})$  with ratio  $\alpha_1$  on the RSNA Bone Age dataset.

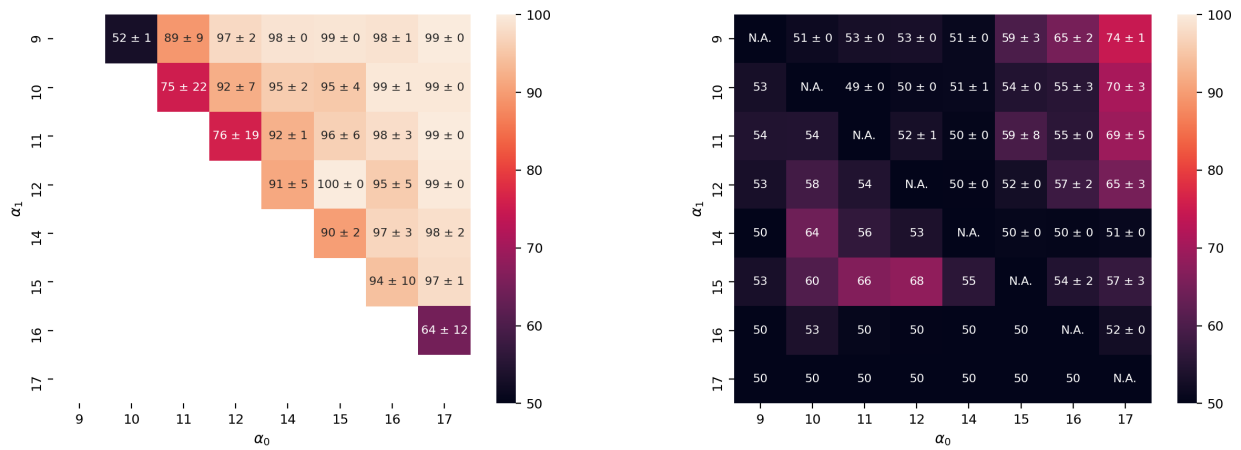


Fig. 12: Classification accuracy using meta-classifiers (left), Loss Test(right, lower triangle), and Threshold Test (right, upper triangle), for distinguishing between training distributions with mean node-degrees  $\alpha_0$  and  $\alpha_1$  on the ogbn-arxiv dataset.

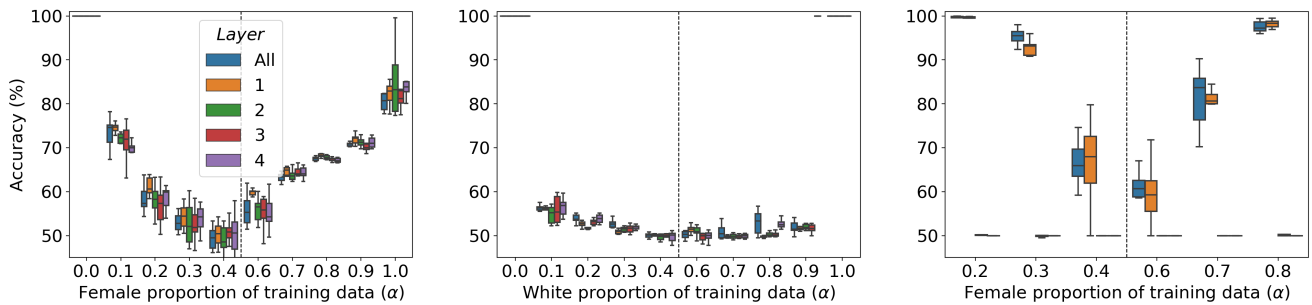


Fig. 13: Classification accuracy for distinguishing between training distributions for unseen models for on Census (sex: left, race: middle) and RSNA Bone Age, while varying the models' layers used while training meta-classifiers.

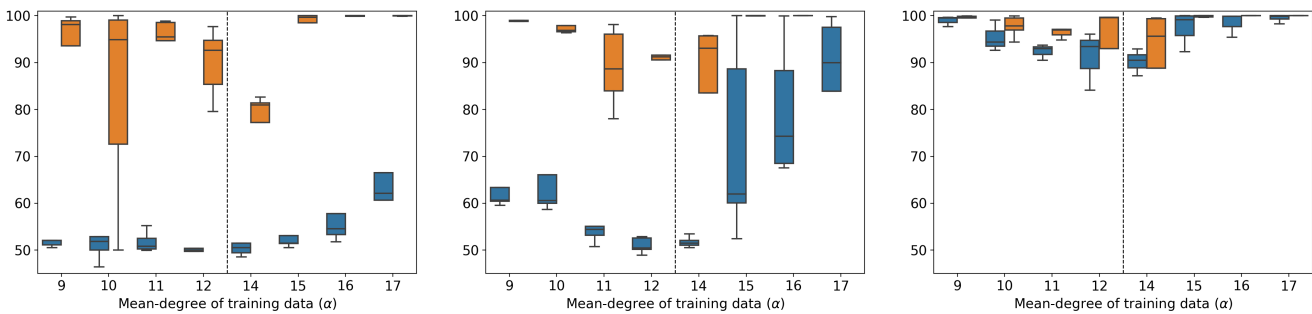


Fig. 14: Classification accuracy for distinguishing between models with different training distributions for on the ogbn-arxiv dataset. Left to right: meta-classifiers trained using 20, 100, and 1600 (original experiment) models, respectively. Orange box plots correspond to using parameters only from the first layer, while blue box plots correspond to using all (three) layers' parameters.



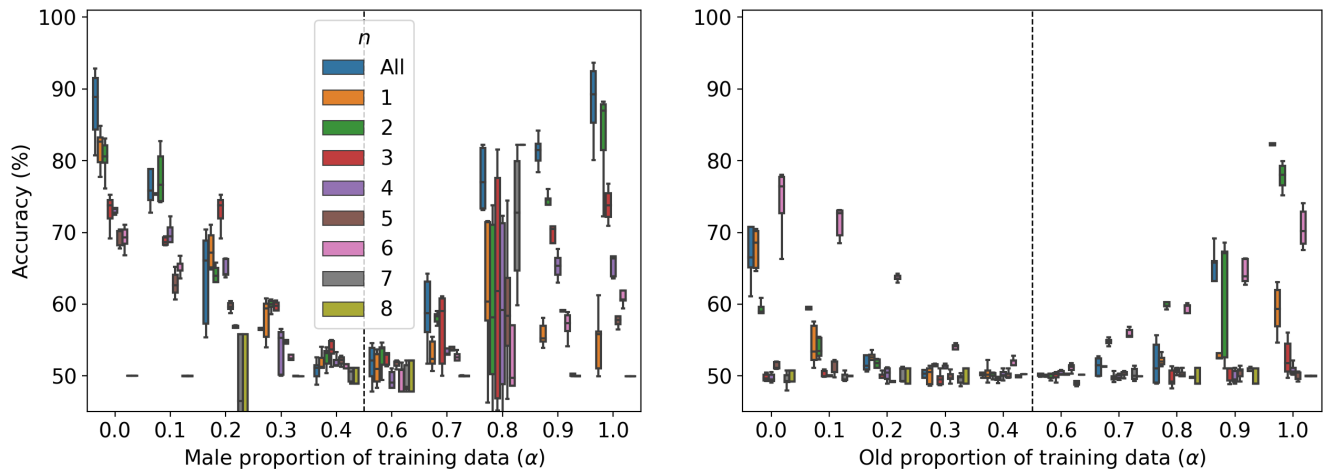


Fig. 15: Classification accuracy for distinguishing between training distributions for unseen models for CelebA (females: right, old people: right) and RSNA Bone Age, while varying the models' layers used while training meta-classifiers.